University of Padova

Italian summer school final report

The CMS Phase II Outer Tracker Upgrade at Fermilab

Supervisors:

Lorenzo Uplegger

Fabio Ravera

Student:

Nicolò Salimbeni

Academic year 2022/2023

Contents

Introduction

Abstract

The Large Hadron Collider (LHC) will be upgraded to increase the instantaneous luminosity up to $5-7.5\times10^{34}\text{cm}^{-2}\text{s}^{-1}$. To face these challenging conditions the CMS tracking system must be updated, using modules that on the one hand are able to cope with high radiations and on the other hand can provide information to the L-1 trigger selection. This report describes the results of some tests on the new tracking modules at the FNAL test beam facility. In particular half of one module was irradiated by 400 MeV protons (total fluence comparable to the one expected through the lifetime of the experiment) and then some analysis were performed on both the irradiated and not irradiated side of the detector with a 120 GeV proton beam. In this report, the efficiency and noise occupancy analysis are presented, with focus on the main critical issues encountered.

1.1 Introduction to LHC and CMS

The Large Hadron Collider (LHC) is the world's largest and most powerful particle accelerator, located at CERN (the European Organization for Nuclear Research) near Geneva, Switzerland. It is a proton-proton collider of 27 km of circumference 100 m underground. In the ring there are four interaction points: CMS, ATLAS, ALICE and LHCb. We are currently in the so called Run 3, with beams colliding at a center of mass energy of 13.6 TeV, expected to collect a total integrated luminosity of 450 fb^{-1}.

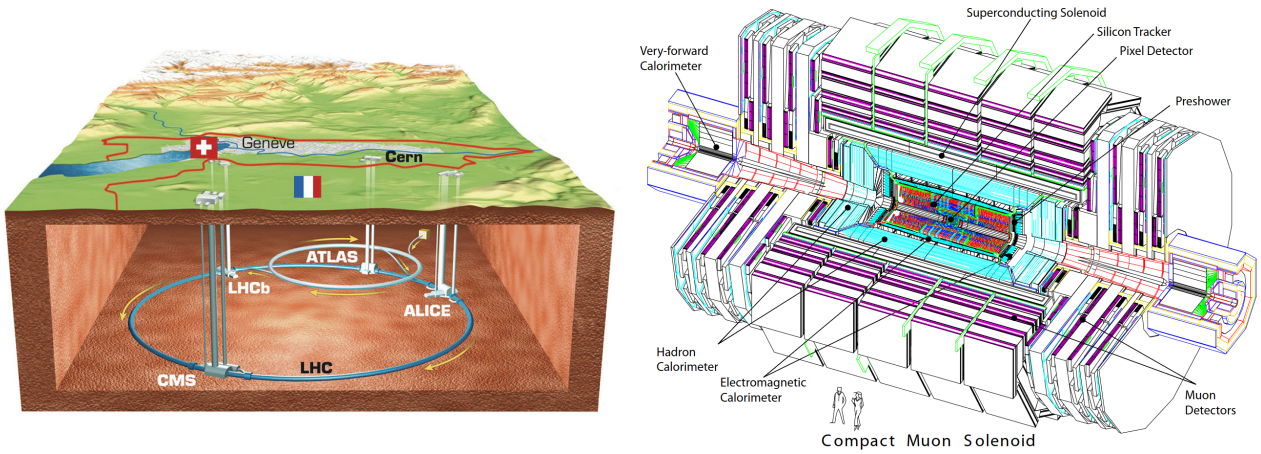

Figure 1.1: on the left a brief scheme of LHC, on the right one for the CMS experiment.

The Compact Moun Solenoid (CMS) is a multi layer detector built with the following goals: the search for the Higgs Boson (accomplished in 2012), the experimental validation at high energies of the standard model and the possibility to discover new physics.
Collisions take place in the center of the detector, and than the interaction point is surrounded by various layers of sensors:

- Tracking volume: 5.8 m long, 2.6 m diameter;

- E.M. calorimeter: made of $PbWO_4$ crystals of 25 $\chi_0 \approx 22$ cm, divided in barrel and endcaps
- Hadronic calorimeter: brass/scintillator sampling calorimeter of 7-11 λ_I;
- Muon chambers outside the solenoid

According to the plans from 2026 LHC should enter the high luminosity phase, where the collisions will take place at 14 TeV, and the integrated luminosity will be between 3000 fb^{-1} and 4000 fb^{-1}. These new setup puts our detectors in very challenging conditions, in particular the amount of collisions each second that takes place will be increased, so the trigger system has to manage much more data, and as a consequence the detectors themselves have to survive to much more charged and neutral particles.

1.2 Focus on the new outer tracking system

The outer tracker will be made out of two types of p_T modules. These new modules are made of a "sandwich" of two silicon detectors parallel to each other and separated by a few millimeters gap. They are called **PS** module and **2S**: the 2S module consists of two strip sensors, each with two columns of 1016 strips and with single cell size of 5 cm $\times$ 90 μm; the PS consists of one silicon micro-strip sensor organized in two columns of 960 strips each with dimensions of 2.5 cm $\times$ 100 μm, and a macro-pixel sensor with a matrix of 32 $\times$ 960 pixels with a pixel size of 1.5 mm $\times$ 100 μm.

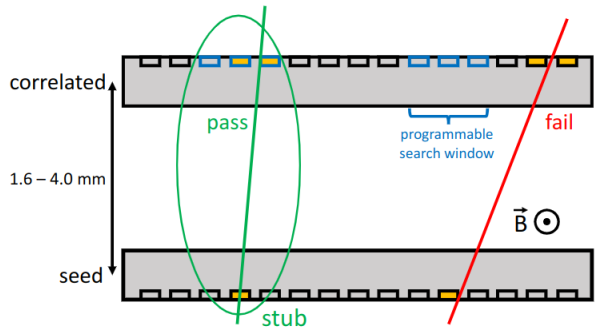

Figure 1.2: illustration of the p_T module concept. Correlation of signals in closely spaced sensors enables rejection of low-p_T particles. The channels shown in green represent the selection window to define an accepted stub; a low-p_T rejected track is shown in red.

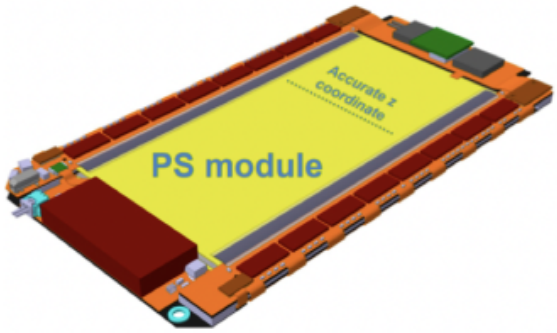

Figure 1.3: on the left a brief scheme of LHC, on the right one for the CMS experiment.

When a particle hit the lower sensor (seed sensor) a window in the upper one (correlated sensor) is opened, then the particle is selected only if it hits the upper window. Since the angle of the track is a function of the magnetic field (known inside CMS) and p_T, selecting different windows we can accept only particles in a specific range of p_T.

1.3 Experimental setup at Fermilab

Now at Fermilab the PS modules are under test. In particular one module was irradiated with 400 MeV protons at the Irradiation Test Area (ITA) at Fermilab and then tested in the Fermilab Test Beam Facility (FTBF) with a 120 GeV proton beam.
Figure 1.5 shows the tracking telescope available at the FTBF and the mounting position of the PS module under test. The detector under test (DUT) was mounted on a remotely controlled rotation platform. Since the facility does not have a magnet to emulate the curvature of the trajectories, the detector must be rotated by a certain angle β. Then a chiller is necessary to keep the irradiated device cold to minimize the sensors annealing.

The track reconstruction and telescope alignment processes are executed using a specialized software package called Monicelli [3]. This package employs a Kalman filter fit to determine the coordinates

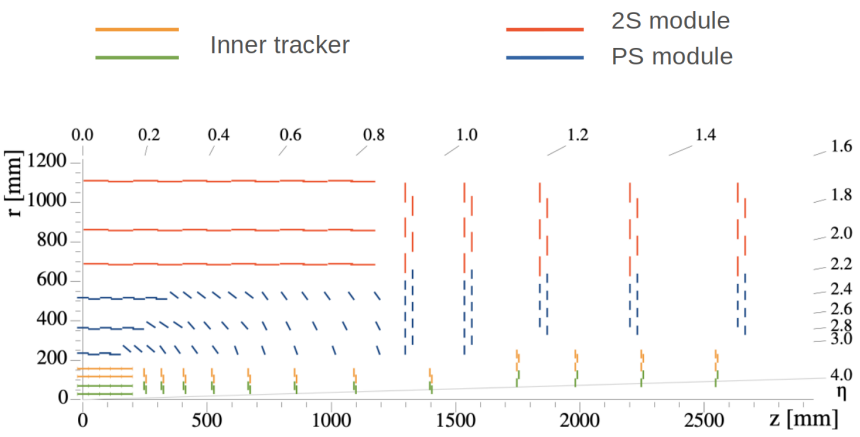

Figure 1.4: sketch of one quarter of the tracker layout, the interaction point is in (0,0)

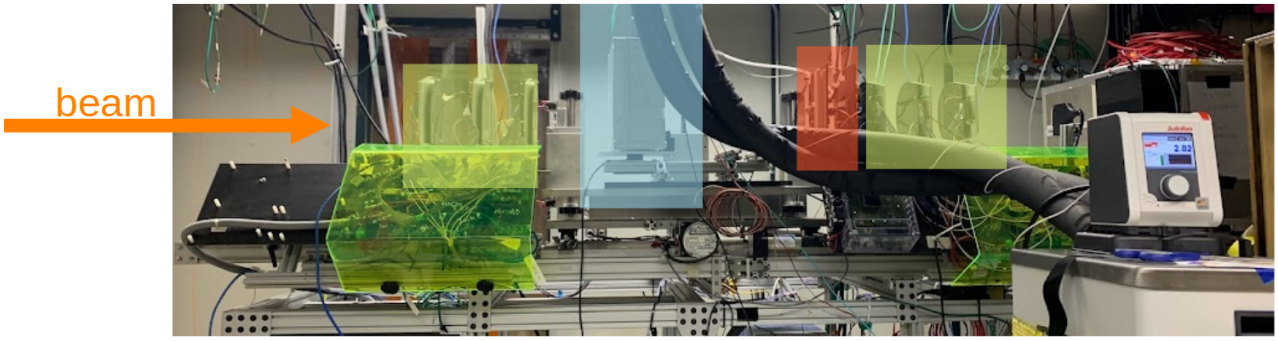

Figure 1.5: tracking telescope available at the FTBF, detector under test (DUT) in the middle (light blue); than in the upstream and downstream positions 12 strips sensors grouped in 6 stations, 3 before 3 after the DUT, of 2 sensors at 90° one with respect to the other (light green); and 2 pixels sensors in the downstream position (light red).

of hit arrays, which have been previously selected based on their proximity (within $\pm 500; \mu$m) to a straight line connecting a hit on the initial plane and one on the final plane of the telescope. In instances where clusters of adjacent pixels or strips are present, the hit coordinates are computed using the linear relationship established between the relative charge shared by these elements and the hit's proximity to their boundary. This linear relationship was established during the telescope's initial commissioning phase, and errors associated with the coordinates were also calibrated during this period. The telescope resolution is around 6 μm - 7 μm for most of the tracks.

1.4 The detector under test

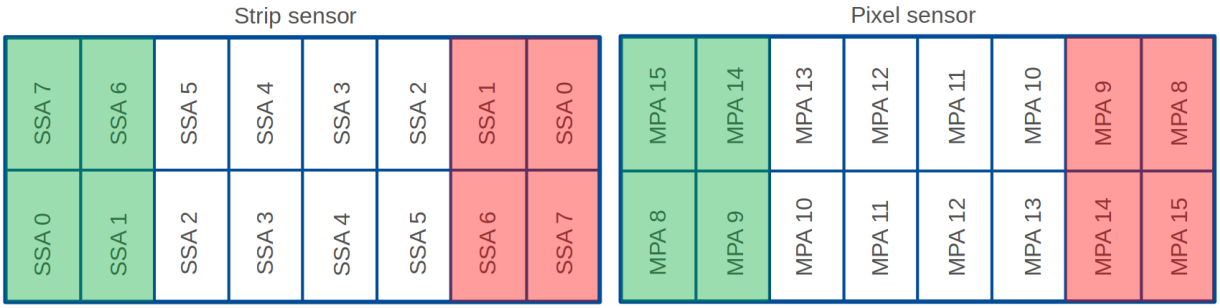

Figure 1.6: on the left the scheme of a strip sensor, one the right of a pixel sensor. Not irradiated chips are marked in green, while fully irradiated chips in red

As previously mentioned, the PS module is composed of two sensors: a strip sensor made of two rows

of 960 strips each, a pixel sensor made of 32 rows and 960 columns of macro pixels. These two sensors contain 16 separate read out chips each. Macro Pixel ASICs (MPA [2]) are used for the pixels, while Short Strip ASICs (SSA [1]) are used for the strips.
These chips are placed in a 2×8 matrix and labelled like in figure 1.6.
As mentioned previously, half of the chip was irradiated. Unfortunately the irradiation is not perfectly uniform, consequently from now on when we refer to irradiated chips we will mean the chips in red, while for non-irradiated chips those in green. The central chips, however, were not considered in the analysis presented in this report.

Study of the efficiency of the detector

2.1 Sensors efficiencies introduction

To calculate the efficiency of the sensors the basic idea is simple: using the telescope it is possible to know when a particle passes inside the detector, at this point it is enough to check that the expected hit is present.
To do this, however, there are some complications. The beam does not send the protons exactly one by one, therefore to bring us back to the case described previously it is necessary to make some cuts on the events. The cuts applied in selecting the traces are the followings.

- In the telescope there are a total of 16 detecting planes and it is required that in at least 13 of them there is only one hit. In this way we are almost sure that just one proton passed though the detector under test;
- To be sure that the trace has been reconstructed well by Monicelli only the cases in where $\chi^2/\text{NDOF} < 5$ are accepted;

2.2 Sensors efficiencies for not irradiated side

Let's see the results of what was obtained for the non-irradiated side of the sensors using the strategy described previously. The results are in fig. 2.7 for pixels and in fig. 2.8 for strips.

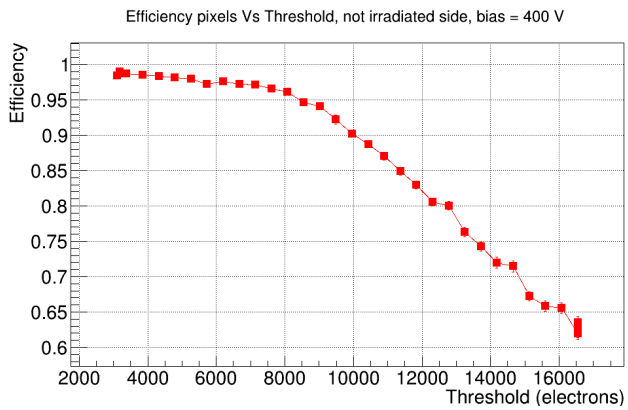

Figure 2.7: pixels sensor efficiency as a function of the threshold for not irradiated chips.

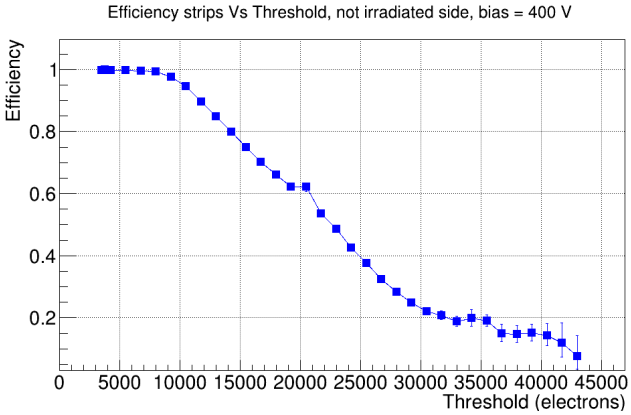

Figure 2.8: strips sensor efficiency as a function of the threshold for not irradiated chips.

First we must specify that the conversion used to have the electrons on the x axis instead of the threshold measured in daq units of the readout chip was provided by a previous analysis. It will not be explored in detail in this paragraph for reasons that will become clear later. For further information on this topic, refer to the dedicated section 4.1.
Regarding the graphs, both show the expected trend. The efficiency decreases as the threshold increases because as it rises, some protons don't create enough charge in the sensor to pass the threshold and thus they are not detected. But there is something that should be noted. For silicon pixel or strip

detectors the expected efficiency at low threshold should be approximately 100%. But as you can see in figure 2.7 for pixels it starts slightly below, around 98.5%.

2.3 Pixels efficiency in more details

The first thing we did was take some data sets with a lot of statistics and see in two dimensions if the efficiency was homogeneous across the entire detector. The resulting plot is in figure 2.9.

The 2D efficiency map has a lot to say about the problem. First of all it is possible to see how in most of the surface the efficiency is practically 1, as expected. Furthermore, the inefficient areas are not distributed randomly but have a well-defined geometric pattern. All this raises the suspicion that there are no errors in the data acquisition or analysis, but there is probably something in the design of the sensor.
Indeed this is the case. Looking at the pixel design fig. 2.10 and 2.11 you can see two grounded structures not connected to the readout system. These, being at the same voltage as the readout chip, also collect charges, charges which are then not detected by the electronics.

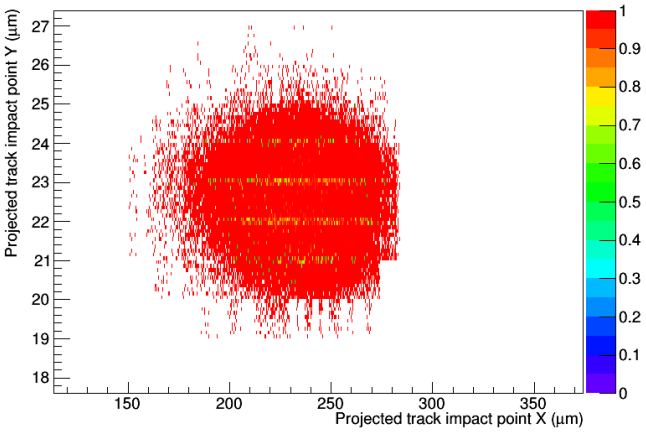

Figure 2.9: 2D efficiency map with the beam pointing in the not irradiated side, the inefficiency shows a clear geometrical pattern.

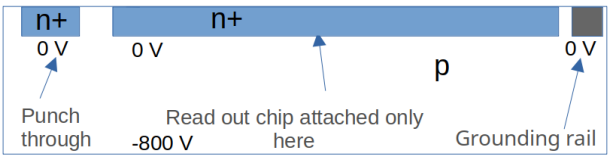

Figure 2.10: vertical section of one pixel. There are 3 components at 0 V but just one is connected to the readout chip.

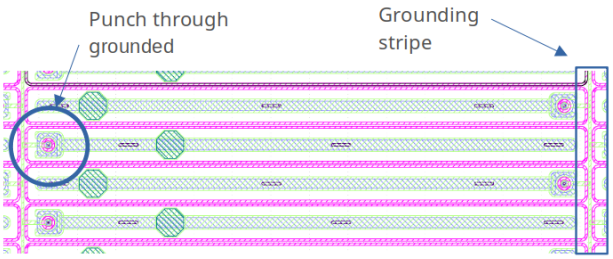

Figure 2.11: design of the pixel sensor from above, there are 2 grounded structures: the pouch through and the grounding stripe.

At this point the last thing to do to confirm the thesis is to print the 2D efficiency map again, but with a much higher resolution, hoping to see the inefficient areas in the same position as the grounded components. Figure 2.12 confirms that the inefficiency is due those components so it is possible to conclude that the efficiency obtained is consistent with the sensor used.

2.4 Sensors efficiencies for not irradiated side

At this point it is possible to move on to study the efficiency in the case of irradiated sensors. Using the same procedure described for the graphs in the non-irradiated chips (fig. 2.8 and fig. 2.7) the following results are obtained, figures 2.13 and 2.14.
Let's start by first discussing what is expected. Radiation causes damage to the crystal lattice of silicon sensors. Mainly, so-called "traps" are formed for the moving charges. Free electrons are trapped for a certain period of time and then start their motion again driven by the electric field of the bias voltage. Generally, to mitigate this effect the electric field must be increased, and in fact we have gone from a bias of 400 V to a bias of 800 V. In any case, however, the negative effects are not completely eliminated. Compared to the non-irradiated case, it is reasonable to expect a loss of efficiency of

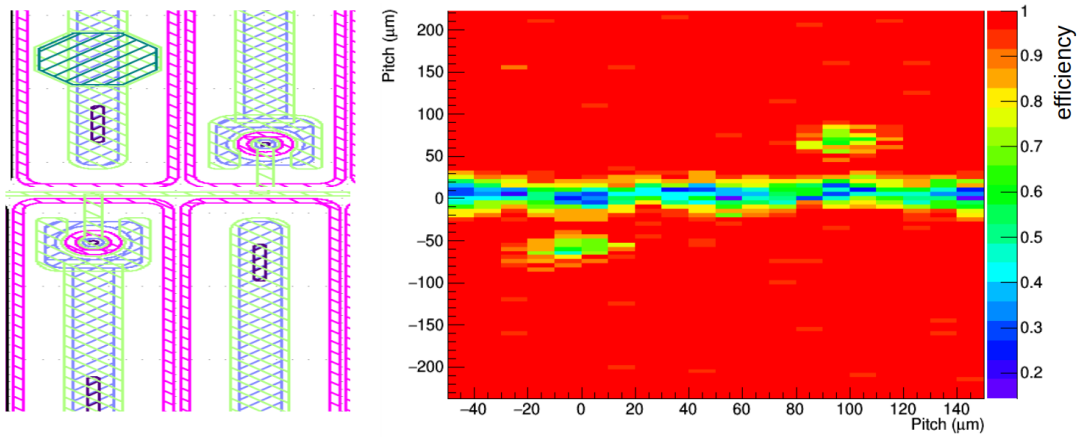

Figure 2.12: close op of the 2D efficiency map near two punch throughs and a grounding rail. On the left the sensor design, on the right the same spot in the 2D efficiency map.

1%-2% at a low threshold, while as the threshold increases it is reasonable to observe a much more sudden drop with respect to the previous case.

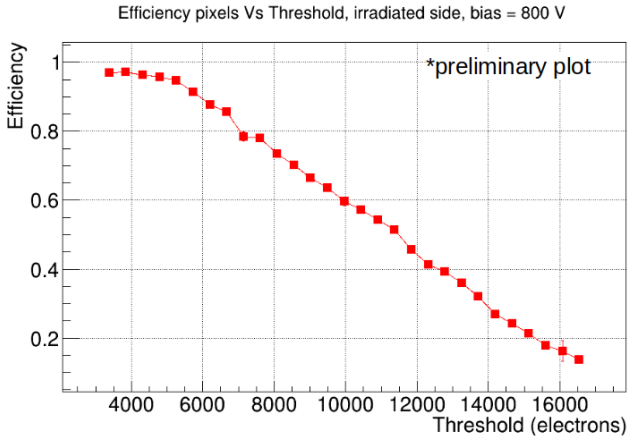

Figure 2.13: pixels sensor efficiency as a function of the threshold for irradiated chips.

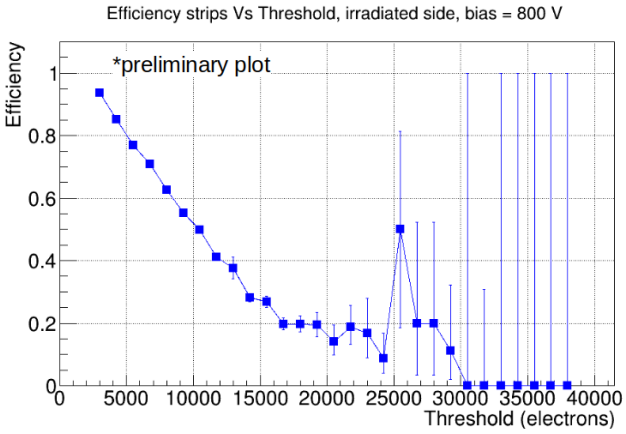

Figure 2.14: strips sensor efficiency as a function of the threshold for irradiated chips.

Now the pixels behave as expected, the efficiency at low threshold has gone from 98.5% to around 97%, while at high threshold this value drops as expected.
Instead, it is the strips that behave unexpectedly. In the non-irradiated case the efficiency was close to 100%, while in the low-threshold irradiated case it starts from around 93%. Furthermore, it does not present an initial plateau like in all the graphs shown so far, but drops quickly as the threshold starts to increase.
Experimentally this is a very serious problem, if the efficiency drops too much it becomes difficult to effectively select the desired events. In fact, remember that in the final setup a particle will be used in the first level trigger only if it leaves a detectable trace both in the pixel sensor and in the strip sensor. Therefore it is important to have a higher efficiency value.
Before making these considerations, however, it is necessary to also take into account how the noise of the detector varies as the selected threshold varies. This is the topic of the next chapter, after which we will delve into this unexpected behavior of the strip sensor.

Noise occupancy characterization

3.1 What is the noise occupancy and how we estimate its value

Noise occupancy is usually defined as:

$$\text{pixel/strip noise occupancy} = \frac{\text{number of hits in one pixel or strip}}{\text{number of triggers}} \tag{3.1}$$

And ideally we would perform this analysis pixel by pixel (strip by strip) but it is not possible since we don't have enough statistics, what we do instead is:

$$\text{module noise occupancy} = \frac{\text{total number of hits}}{\text{number of triggers} \times \text{number of pixels (strips) in the detector}} \tag{3.2}$$

3.2 Noise occupancy estimation

At this point we build an histogram like the one in fig. 3.15

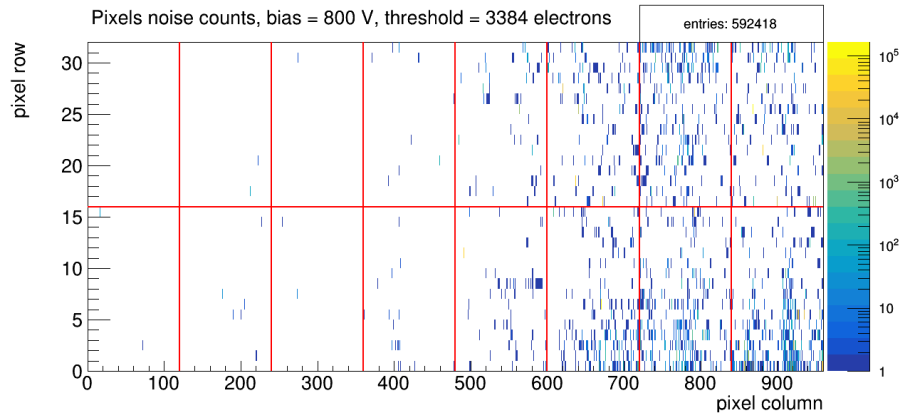

Figure 3.15: hit map for a the pixel sensor without beam, only noise counts, with almost 2300000 triggers.

In this context, we utilize a 2D histogram in which each bin represents an individual sensor pixel or strip (in this case, pixels, although we also created a similar graph for strips). The count in each bin corresponds to the number of noise events observed for that particular pixel.
Due to the irradiation of the readout chips on the right side, we are compelled to partition the detector into sections based on the irradiation level. As previously mentioned, the right side comprises four fully irradiated chips, while the left side consists of four non-irradiated chips. Given that the noise distribution significantly varies with the degree of damage, our analysis will concentrate solely on these two scenarios, excluding the eight chips in the middle, which experienced non-uniform irradiation. Figure 3.15 illustrates, as anticipated, that the majority of noise is concentrated on the irradiated side. Furthermore, within this region, most sensors exhibit minimal noise counts, typically fewer than 10. Nevertheless, a noteworthy issue arises: certain pixels exhibit noise counts exceeding 10^5 (hereafter referred to as "noisy" pixels for brevity). Clearly, this level of noise is not acceptable given a dataset of 2×10^6 triggers, as the noisy pixels would contribute to an occupancy of nearly 5%. These noisy pixels deviate from the expected behavior, prompting us to consider their exclusion from the analysis. However, we face the challenge of establishing a robust criterion for identifying a pixel as "noisy."

3.2.1 How to exclude pixels from the analysis

We established that we could tolerate a module noise occupancy of up to 10^{-6}. With this criterion in mind, we proceeded as follows: we considered the most unfavorable scenario, involving the highest bias voltage, the lowest threshold, and exclusively irradiated chips. In this context, we needed to determine an upper limit for the number of noise counts above which a pixel would be classified as "noisy" and consequently excluded from the analysis. To address this, we generated a plot depicting the noise occupancy of the irradiated side as a function of this limit, which dictates when a pixel is deemed noisy and excluded from consideration. This approach led to the creation of the graph presented in figure 3.16:

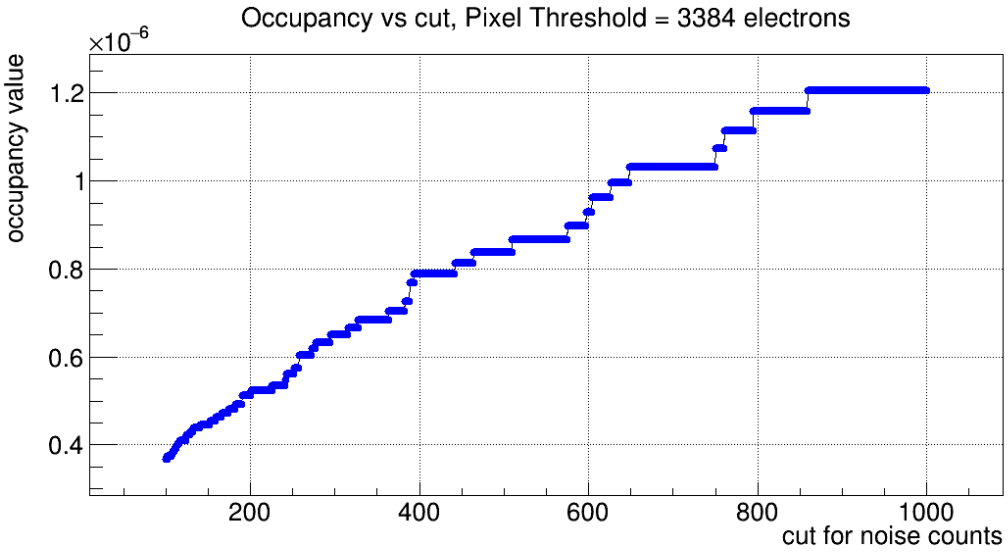

Figure 3.16: occupancy value only for the irradiated side as a function of the maximum number of hits accepted for a pixel.

As anticipated, the occupancy value demonstrates a clear trend: when the cut is set low, meaning the maximum permissible number of counts in a single pixel is stringent, a substantial number of pixels are excluded from the analysis, resulting in low occupancy. Conversely, when we raise the cut, allowing for a higher upper limit, a greater number of noisy pixels are included in the analysis, leading to higher occupancy. At this juncture, we must determine the maximum allowable count value in each pixel according to our specific requirement. Referring to Figure 3.16, and given our chosen maximum noise occupancy of 10^{-6}, we should exclude all pixels with more than 650 noise counts. However, due to a small plateau observed just before the 10^{-6} occupancy level, we opted for a cut-off at 600 counts. Consequently, moving forward, any plot featuring noise occupancy in this report will be computed with the exclusion of all pixels or strips with more than 600 noise counts. Now, a pertinent question arises: how many pixels/strips are we excluding? In the worst-case scenario, we are excluding 40 out of 30,720 pixels and 3 out of 1,920 strips, representing 0.13% and 0.15% of the total, respectively. Given that the trimming procedure, is already masking around 1% of the pixels (due to them being untrimmable), an additional exclusion of 0.13% for pixels is not substantial. Moreover, the strips experience an even more favorable outcome, as the 0.15% excluded sensors represent the only ones excluded in this case.

3.3 Unexpected noise for strips

In fig. 3.15 we saw the 2D hit map for the pixel sensor, below the strips one is reported:

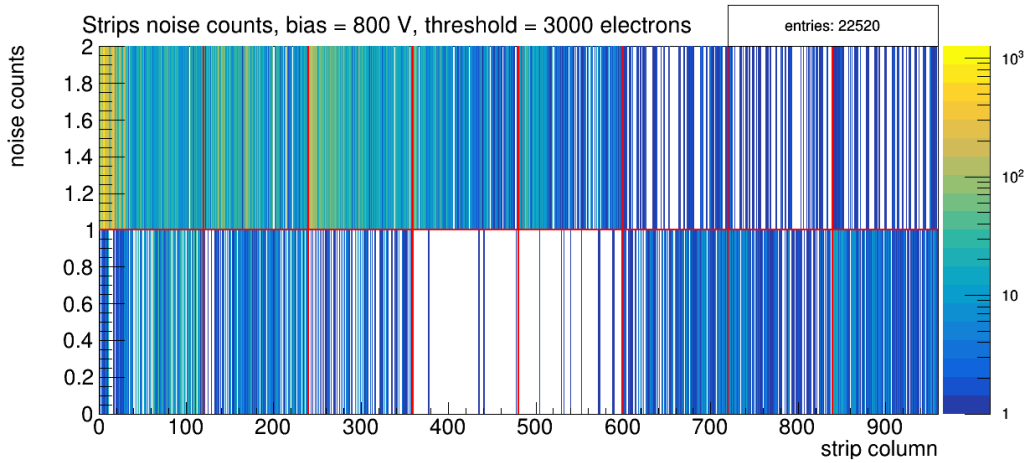

Figure 3.17: hit map for strip sensor without beam, only noise counts, with almost 2300000 triggers and low threshold.

There we can notice a very unexpected behavior, on the not irradiated side of the sensor the noise occupancy is higher than on the irradiated side. But then when we increase the threshold we get:

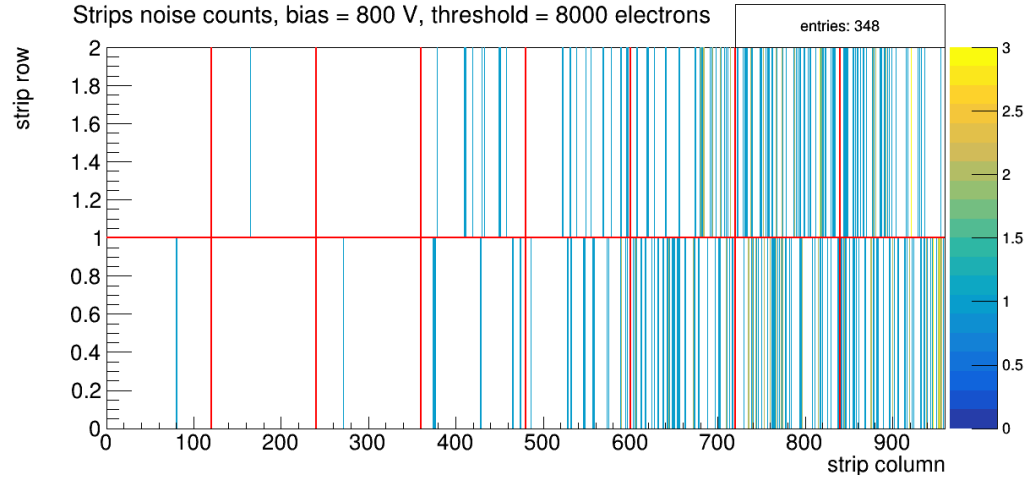

Figure 3.18: hit map for strip sensor without beam, only noise counts, with almost 2300000 triggers and high threshold.

This indicates that there is an external source of noise affecting the left side of the sensor. However, this noise can effectively be mitigated by employing a higher threshold.
Upon reviewing the module's design, we identified that the DC/DC converter is located on that particular side of the module, which is likely the source of the injected noise. In any case this issue was not studied further as it had already been reported in previous reports and considered not significant for the studies to be undertaken.

3.4 Noise as a function of the threshold for pixel and strip sensor

After having explained how the noise was defined, how to exclude excessively noisy channels, and having justified the unexpected behavior of the strips, it is possible to draw the graph (threshold, noise occupancy) we were looking for, both for the irradiated and non-irradiated side of the sensor: fig. 3.19.
In these graphs, taking into account what was said previously, everything behaves as expected. First

of all, the noise occupancy decreases as the threshold increases, explaining intuitively: if the threshold is higher it is less likely that a noise signal (usually very low) will exceed it.
Secondly, the noise on the irradiated side is higher than the noise on the non-irradiated side. Here too, as expected, if the silicon lattice is damaged it is more likely that an electron will leave the valence band and go to the conduction band. What has just been said is always true for high thresholds, while for low thresholds this is not the case for the strips as the DC/DC converter in this case considerably increases the background noise.
Another thing that confirms the validity of the analysis carried out is that the lowest threshold point of all for the pixels is found exactly below the maximum value decided for the module occupancy of 10^{-6}. It couldn't be otherwise given that the maximum limit of 600 counts was chosen specifically for this.

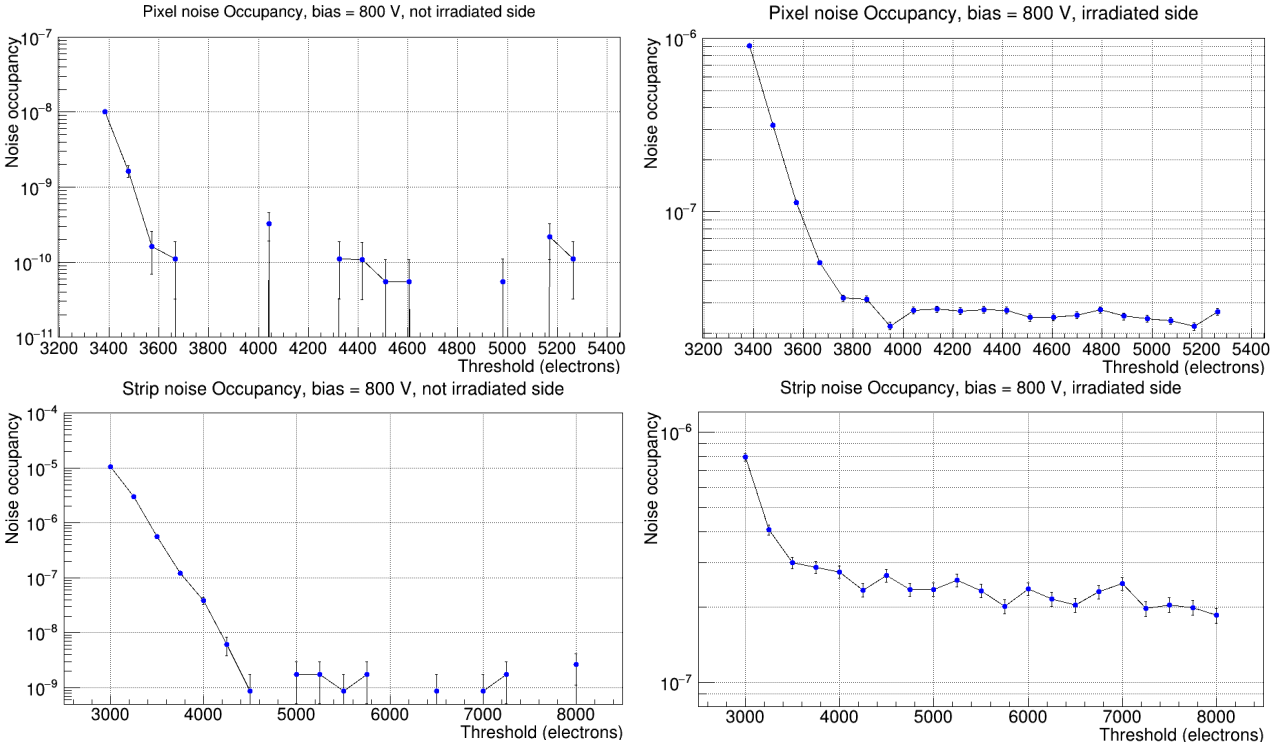

Figure 3.19: module noise occupancy as a function of the threshold for both pixels (up) and strips (down) in the not irradiated (left) and irradiated (right) side.

Finally, a final comment is necessary regarding the graphs of the non-irradiated side. In these you may notice "holes" as the threshold has been raised. Those points are exactly zero and cannot be represented in a logarithmic scale. Please note, this does not mean that in these conditions the detector has no background noise, it only means that not enough statistics have been collected to detect it. Since we are studying counts, which follow a Poissonian distribution, occasionally if the expected value is almost 0 it is possible not to obtain any counts.

3.5 Noise and efficiency during the testbeam

At this point of the analysis it is possible to study the efficiency in relation to noise with more awareness. This is very important, as ideally you would like the highest possible efficiency and at the same time zero background noise. This is obviously not possible, to increase efficiency it is necessary to lower the threshold, so as to detect even the smallest signals. Doing this, however, necessarily increases the probability that a noise signal will cross this threshold, generating a dark count.
What we need to do at this point is put ourselves in a position to consciously balance the two things. So the four following graphs in figure 3.20 were printed. In these four, one presents a non-negligible criticality, in the irradiated case for the strips the efficiency starts from a fairly low value, around 94%. This means that there are two main possibilities: choosing the lowest possible threshold but having a

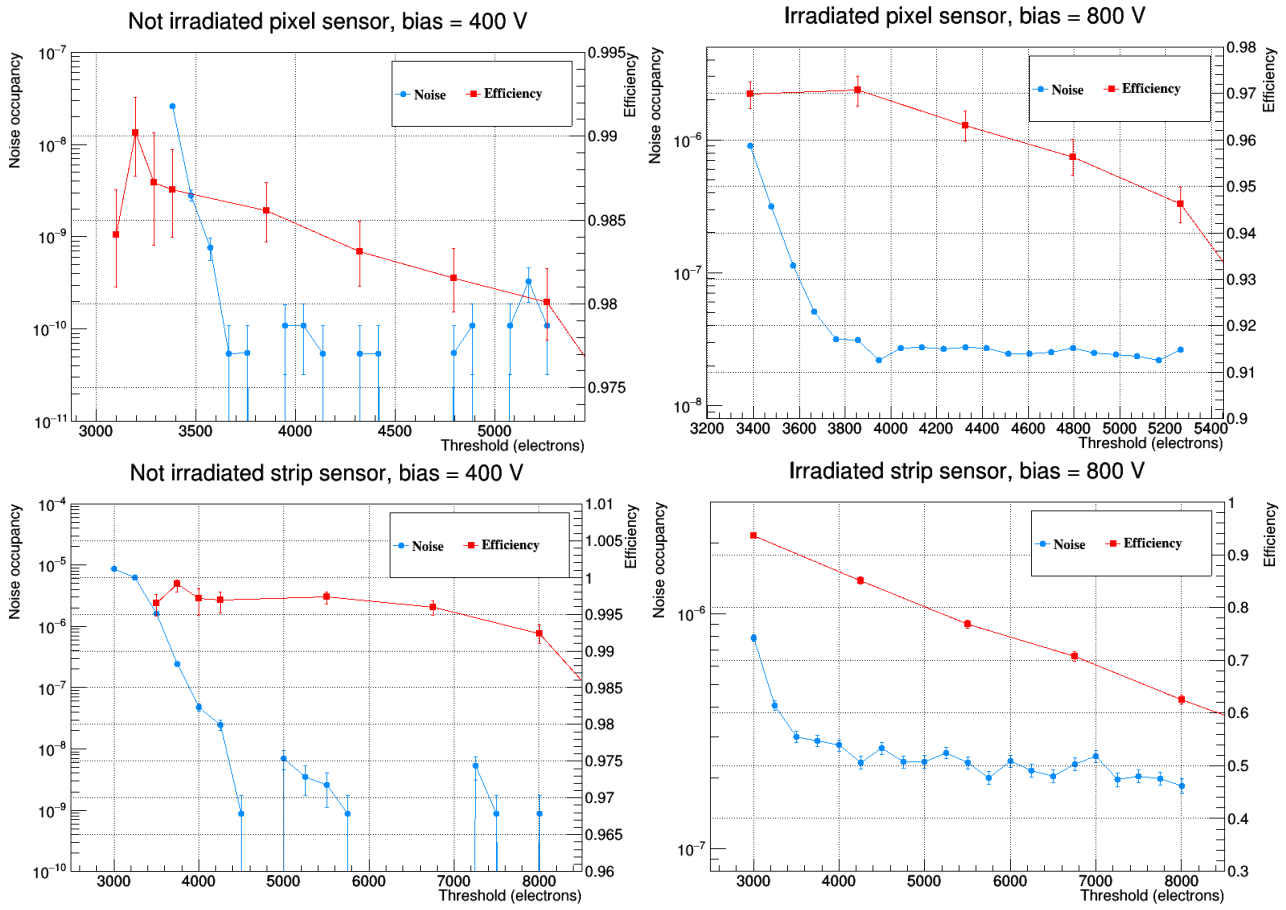

Figure 3.20: module noise occupancy and efficiency as a function of the threshold for both pixels (up) and strips (down) in the not irradiated (left) and irradiated (right) side.

very high background noise, or choosing an higher threshold, therefore having little noise, but greatly sacrificing efficiency. Due to unexpectedly low values of efficiency at high thresholds, one is forced to choose the lowest threshold studied at the expense of the noise that will increase.
This behavior is so unexpected that one of the plausible explanations is having made an error somewhere during the data analysis. This will in fact be the topic of the next chapter.

Threshold settings

Before delving deeper into the topic, it is necessary to understand what it means and what purpose it serves to convert the threshold from daq units to electrons. To select the signals you need to set a threshold that is high enough to exclude noise but low enough to accept even the small signals generated by the particles. The threshold is set once in each readout chip using an internal register. In practice the value of this register can be measured in "daq units", and each unit increases the threshold value by a little. At this point it is necessary to know what a single unit of daq corresponds to, so as to be able to understand its physical meaning. The idea is to convert the daq units into electrons so that we can reason as follows: if I want to accept all the particles that release more than n electrons in the detector I must know how many n electrons are in daq units and then set the threshold to this value in the register. Now let's first see how to interpret the threshold, and then how to convert it appropriately into electrons.

4.1 Convert daq units to electrons, old strategy

To calculate the conversion from daq units to electrons we used an injected charge.
Before starting, a clarification is necessary: by convention from now on the daq units of the register in the readout chip will be measured in "Vth" while the injected charge is measured in "Vcal".
The first thing to do is to measure the base level of the electronics which we will cal "pedestal", as each measured signal will be the sum of the charge released by the particle added to it. So if you want to measure the threshold in collected electrons it will be necessary to know the value of the baseline from which to start.
To better understand the situation, let's see an example signal in figure 4.21:

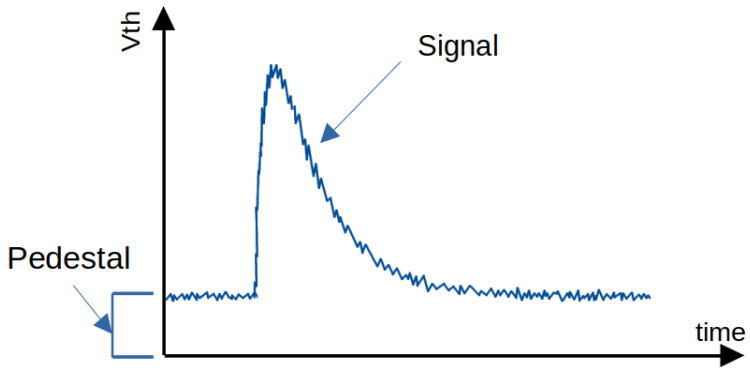

Figure 4.21: example of pedestal and signal in the readout chip.

4.1.1 Pedestal estimation

To find the pedestal of each pixel/strip we used a constant injected signal in the readout. Then by doing a threshold scan we obtain an S curve whose value at 50% occupancy corresponds to the sum of the injected signal plus the pedestal. The following example is for a strip, but the procedure is the same for pixels.

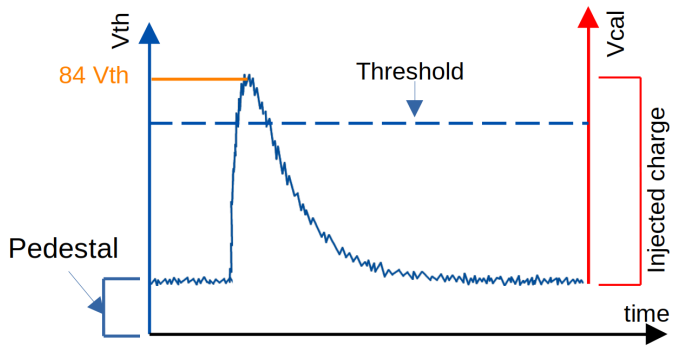

Figure 4.22: Injected charge plus pedestal for a specific channel.

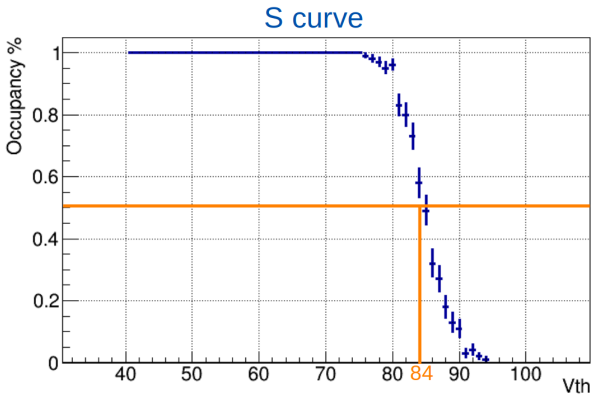

Figure 4.23: S curve obtained for a single channel (strip or pixel).

Since we know the conversion into electrons for both Vth and Vcal it is possible to find the pedestal[1].

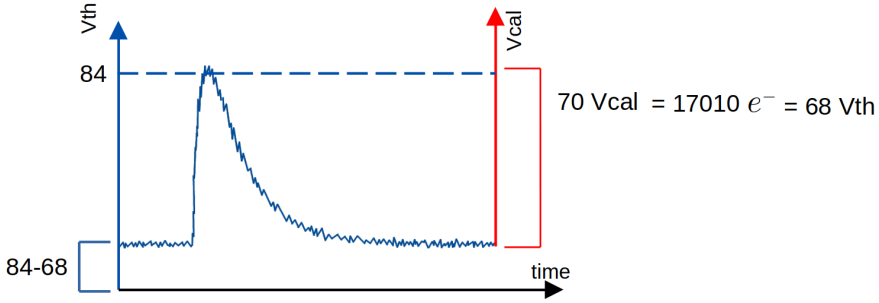

Figure 4.24: pedestal estimation for a single strip.

MPA	
1 Vcal	220 e^-
1 Vth	94 e^-
SSA	
1 Vcal	243 e^-
Vth	250 e^-

Table 4.1: known conversion from Vcal and Vth into electrons.

In this specific case the pedestal is 16 Vth, so when you want to calculate the threshold in electrons the calculation to be done will always be the following (for strips): $(\text{Vth} - 16) \times 250\ e^-$.
A clarification is necessary here, the process done to achieve this result only takes into account one channel (whether strip or pixel). In the sensor there are 120 strips for SSA and 120 $\times$ 16 pixels for MPA. To generalize the process simply instead of taking the maximum of a single channel (in the example 84 Vth) a histogram is constructed with the distribution of all the maximums and then the average is taken.
Now it is good to make a clarification, the conversion values reported in the 4.1 table were calculated in previous studies and used here as an assumption.
A possible explanation for the inefficiency of the strips observed previously is that we were using a threshold higher than expected. When the data was taken the first point was expected to be at 3000 electrons, but maybe, if the conversion was wrong, the real threshold was actually higher.
To test this hypothesis, a more sophisticated method for the conversion from Vth to electrons was used, which now only assumes that the conversions from Vcal to electrons are correct (this assumption is reasonable given how the charge injection system is built).

4.2 Convert daq units to electrons, new strategy

We measured the average mean value of the SCurves as a function of the injected charge in each sensor, then using a linear fit it's possible to have a new conversion. The idea is to find a direct relationship between Vth and electrons, without having to go through the pedestal calculation. Results in figure 4.25. The choice of the fit is not free from compromises, ideally the points collected should be perfectly linear as the more charge you inject, the higher Vth must be. From the points, however, the linear trend is not perfectly respected, this could be due either to a non-linearity of the response of the

[1]We get the same values for irradiated and non irradiated detector.

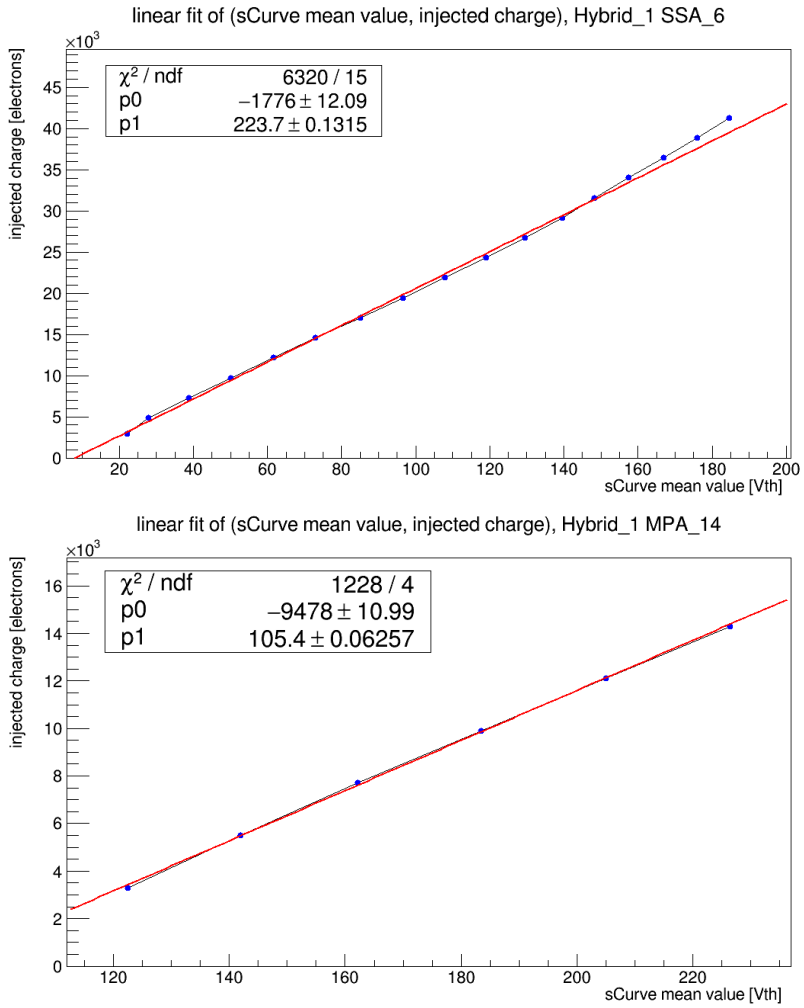

Figure 4.25: Conversion from Vth to electrons for Hybrid 1, SSA 6 (strips) and MPA 14 (pixels)

readout chip (non-linear Vth) or to a non-linearity of the injected charge (non-linear Vcal).
A possible strategy would be to fit the points with a very high degree polynomial, so as to obtain a very precise conversion for the range studied. However, this method cannot always be generalized as the polynomial diverges outside the collected points. So in the end, to have a conversion that was as general as possible, the linear fit was chosen, which although it loses accuracy, can be used on all occasions.
Now let's compare, just in the case of hybrid 1 SSA 6 for brevity, the new conversion with the old one, to understand if there are substantial differences:

- old conversion: 1 Vth = 250 e^- and pedestal at $\approx$ 13 Vth;
- new conversion: 1 Vth = 223 e^- and pedestal at $\approx$ 8 Vth;

For the new strategy the pedestal is calculated as the intersection point between the fit and the x-axis, which corresponds to Vth in the case of 0 injected charge.
The conclusion is that during data collection (using the old conversion) when we believed we were at 3000 threshold electrons, in practice we were at around 3800. This explains the very low efficiency obtained in the graph 2.14.

4.3 Conclusions

First, the efficiency of the detectors as a function of the threshold was studied. In this case, two unexpected behaviors were noted which were first explored and then explained: the pixels do not start

from an efficiency of 100% due to the presence of the punch through and the grounding rail, the strips in the irradiated case seemed to have an efficiency lower than necessary due to the incorrect conversion from Vth to electrons.
The noise was studied at various thresholds, also in this case addressing some critical issues. Some channels were unexpectedly noisy and had to be excluded. To select which ones to exclude, a request was made on the maximum noise occupancy acceptable for the module, and the cut to be applied accordingly was decided. Than moreover for the strips, a noise occupancy higher than expected was noted on the non-irradiated side. This behavior was attributed to the DC/DC converter and by raising the threshold the problem was solved.
Finally, in trying to solve the problem of strips with low efficiency, a conversion from Vth to electrons has also been developed, this new strategy is much more precise than the previous one and must be used to redraw all the graphs already made and for all future analyses.

Bibliography

[1] Alessandro Caratelli, Davide Ceresa, Jan Kaplon, Kostas Kloukinas, Yusuf Leblebici, Jan Murdzek, and Simone Scarfi. Short-strip asic (ssa): A 65nm silicon-strip readout asic for the pixel-strip (ps) module of the cms outer tracker detector upgrade at hl-lhc. *PoS*, TWEPP-17:031, 2018.

[2] D. Ceresa, A. Marchioro, K. Kloukinas, J. Kaplon, W. Bialas, V. Re, G. Traversi, L. Gaioni, and L. Ratti. Macro pixel asic (mpa): the readout asic for the pixel-strip (ps) module of the cms outer tracker at hl-lhc. *Journal of Instrumentation*, 9(11):C11012, nov 2014.

[3] Simon Kwan, CM Lei, Dario Menasce, Luigi Moroni, Jennifer Ngadiuba, Alan Prosser, Ryan Rivera, Stefano Terzo, Marcos Turqueti, Lorenzo Uplegger, Luigi Vigani, and Mauro E. Dinardo. The pixel tracking telescope at the fermilab test beam facility. *Nuclear Instruments and Methods in Physics Research Section A: Accelerators, Spectrometers, Detectors and Associated Equipment*, 811:162–169, 2016.